

Nanoscale

Accepted Manuscript



This is an *Accepted Manuscript*, which has been through the Royal Society of Chemistry peer review process and has been accepted for publication.

Accepted Manuscripts are published online shortly after acceptance, before technical editing, formatting and proof reading. Using this free service, authors can make their results available to the community, in citable form, before we publish the edited article. We will replace this *Accepted Manuscript* with the edited and formatted *Advance Article* as soon as it is available.

You can find more information about *Accepted Manuscripts* in the [Information for Authors](#).

Please note that technical editing may introduce minor changes to the text and/or graphics, which may alter content. The journal's standard [Terms & Conditions](#) and the [Ethical guidelines](#) still apply. In no event shall the Royal Society of Chemistry be held responsible for any errors or omissions in this *Accepted Manuscript* or any consequences arising from the use of any information it contains.

Cite this: DOI: 10.1039/c0xx00000x

www.rsc.org/xxxxxx

ARTICLE TYPE

Graphene-based single fiber supercapacitor with a coaxial structure

Xiaoli Zhao,^a Bingna Zheng,^a Tieqi Huang^a and Chao Gao^{a,*}

Received (in XXX, XXX) Xth XXXXXXXXX 20XX, Accepted Xth XXXXXXXXX 20XX

DOI: 10.1039/b000000x

5 A novel all graphene coaxial fiber supercapacitor (GCS) was fabricated, consisting of a continuously wet-spun core graphene fiber and facilely dip-coated graphene sheath. GCS is flexible, lightweight, strong, also accompanied by a high specific capacitance of 205 mF cm⁻² (182 F g⁻¹) and high energy density of 17.5 μWh cm⁻² (15.5 Wh kg⁻¹). The energy density was further improved to 104 μWh cm⁻², when an organic ion liquid electrolyte was used.

10 Introduction

The integration of electronics and textiles can satisfy the great needs for smaller and portable electronics in practical life.^{1,2} The conventional energy storage devices such as batteries and supercapacitors often consist of heavy current collectors and polymer-bound powder electrochemical active materials in a clumsy button or a spiral wound cylinder, limiting their uses in wearable electronics.³ Recently, researchers have shown that a self-standing assembly of low dimensional (*i.e.* large aspect ratio) nanoparticles can be a nice solution to this issue of energy-storage textiles.⁴⁻¹⁵ Among the electrochemical active nanoparticles, the remarkable combined properties of graphene, such as high specific surface area, high electrical conductivity and lightweight, render it an excellent building block for specific shaped supercapacitors. Graphene fibers have got significant development in recently years, demonstrating their advantages such as strength (0.1-0.5 GPa), flexibility, lightweight (0.1-2 g/cm³),^{16, 17} and electrical conductivity (>10⁴ S m⁻¹), thus very suitable for high performance electronic textiles.¹⁸⁻²⁶ Graphene fiber supercapacitors, consisting of two-ply twisted graphene fibers bound by polymer electrolyte gel, showed a high areal capacitance of 1.7 mF cm⁻².²⁷ All-in-one single fiber supercapacitor has also been fabricated by region-specific laser reduction of a graphene oxide (GO) fiber.²⁸ The latter shows a more defined and integrated structure than the former, but holds a limited specific capacitance, probably because of the high solution resistance in the separating layer consisting of closely-packed GO sheets. Thus a more integrated-structured fiber supercapacitor without compromise in electrochemical performance is strongly required.

40 Here, a novel graphene-based coaxial fiber supercapacitor (GCS) is developed with the two electrodes of a continuously wet-spun fiber as the core and a dip-coated cylinder sheath. Compared with the twisted-structured graphene fiber supercapacitor, the face-to-face structure of the two electrodes favours the low solution resistance in the separator layer of a supercapacitor. GCS holds a high specific capacitance of 205 mF cm⁻² (182 F g⁻¹) and an energy density of 17.5 μWh cm⁻² (15.5

Wh kg⁻¹) based on the cyclic voltammetry (CV) test, much higher than the previously reported parallel aligned graphene fiber (9.4 mF cm⁻²)²¹ and also its analogue-CNT coaxial fiber (8.9 mF cm⁻²)²⁹. Because of the electrical double layer capacitor (EDLC) attribute and well-designed structure, GCS holds almost 100% capacitance retention after 10000 cycles of charge and discharge. The capacitance kept 92% after 100 times of bending. We also applied GCS with organic phase electrolyte to enlarge the energy density to 104 μWh cm⁻².

Results and discussion

Figure 1 has schematically shown the fabrication process and cross section morphology of GCS. The axial graphene fiber (AGF) was assembled by a liquid crystal (LC) wet-spinning technique from GO followed by a chemical reduction (see X-ray diffraction data in Figure S1, the d-space changed from 0.8 nm to 0.33 nm after reduction), according to the method previously reported by our group.¹⁹ The diameter of the produced graphene fiber can be adjusted by the spinning conditions, ranging from 10 to more than 100 μm. A polyvinyl alcohol (PVA) gel layer was then dip-coated on AGF to act as the electron separator between the two electrodes in the supercapacitor. Under optical microscope and scan electron microscope (SEM), a uniform layer of polymer was observed (Figure 2a,b, Figure 3a). Then, the polymer-coated fiber was further dip-coated in GO solution to form a GO gel layer. The sheath becomes conductive after chemical reduction by hydroiodic acid. In the reduction process, ethanol was added in aqueous hydroiodic acid to prevent the dissolution of PVA layer. The thickness of the sheath graphene fiber (SGF) can also be controlled by the dip-coating conditions and coating cycles. In a typical coating process, SGF with 50 μm in wall-thickness was fabricated by 5 times of gel coating. After that, a H₂SO₄/PVA gel electrolyte was coated outside to make an integrated GCS. This kind of coaxial structure is expected to decrease the ion transport length in the separator layer, leading to smaller solution resistance in the assembled supercapacitor, as schematically shown in Figure S5.²⁹

Interestingly, the dip-coated GO gel exhibits LC properties, which was confirmed by polarized optical microscopy (POM) and small angle X-ray scattering (SAXS). Figure 2c,d show the POM images of the PVA-coated graphene fiber before and after GO gel coating. A thick layer (*ca.* 0.28 mm) of GO gel was coated, which displays birefringence-induced bright colour between optical polarizers. This indicates the orientation of GO sheets in the coated GO gel. The shrinking process of GO gel during water evaporation is shown in Figure 2d. GO gel shrunk to continuous and uniform solid sheath. Figure 2e-g show the 2D-SAXS patterns of the origin GO solution, gel-state GO fiber (precursor of AGF) and gel-state GO sheath layer (precursor of SGF), respectively. All the three patterns exhibit asymmetry, indicating the orientation of GO sheets. It is noteworthy that gel-state SGF shows a higher degree of asymmetry than the original GO dope solution. We suggest that when PVA-coated AGF was dipped into the LC GO solution, the separated LC domains in the original GO dope solution were further oriented, leading to higher ordering in the coated gel, just like that in the case of LC wet spinning.¹⁹

The microstructure of GCS was observed by SEM. The side view of SGF presents a surface full of oriented wrinkles (Figure 3b). Figure 3c-f show the cross section morphology of GCS without the outer polymer electrolyte layer, while the cross section SEM images of GCS with the outer layer of polymer electrolyte are shown in Figure S3. Under magnification, a lot of voids are seen in both AGF and SGF. As the surface tension of the solvent can draw the graphene sheets together during the solvent evaporation, we used a low surface tension solvent ethanol ($22.32 \times 10^{-3} \text{ N m}^{-1}$) rather than water ($72.75 \times 10^{-3} \text{ N m}^{-1}$) to wash the wet-state fiber, leading to the formation of numerous voids in the resulting fiber.³⁰ The voids inside the fibers could benefit the effective surface area of the graphene sheets in their electrochemical performance. The PVA layer was *ca.* 10 μm in thickness, which is a common value in commercial supercapacitors.

The total capacitance of GCS (C_t), the capacitance of AGF (C_{AGF}) and the capacitance of SGF (C_{SGF}) hold a relationship as follows:

$$\frac{1}{C_t} = \frac{1}{C_{AGF}} + \frac{1}{C_{SGF}}$$

We can deduce from the above relationship that if C_{AGF} and C_{SGF} share the same value, they can make the best contribution to the total capacitance under a fixed sum mass of the two electrodes.²⁹ The electrochemical performances of AGF and SGF were tested under a parallel alignment, in which two AGF or SGF parallel aligned as the two electrodes with $\text{H}_2\text{SO}_4/\text{PVA}$ as the gel electrolyte.²¹ As shown in Figure 4c and Figure S6, AGF and SGF exhibit a similar mass specific capacitance (C_m) and rate performance. Thus, the linear densities of AGF and SGF were controlled to be the same in the assembly process.

Before electrochemical test, the working section of GCS was swelled in 1M H_2SO_4 solution and then left drying under room temperature for more than 24 hours. CV, galvanostatic charge-

discharge (GCD) and electrical impedance spectroscopy (EIS) test were conducted to measure the electrochemical performance of GCS. Figure 4a shows the CV curves of GCS from 10 to 200 mV/s. Under 10 mV/s scan rate, the CV curve of the GCS is axisymmetric and of nearly rectangle shape which indicates the good EDLC property. The calculated areal capacitance (C_A) reaches 205 mF cm^{-2} (the corresponding C_m is 182 F g^{-1} and length specific capacitance (C_L) is 4.63 mF cm^{-1}), note that the areal mass loading³¹ is 2.25 mg cm^{-2} in terms of AGF surface area). The corresponding area specific power density (P_A) and energy density (E_A) are $819 \text{ }\mu\text{W cm}^{-2}$ and $17.5 \text{ }\mu\text{Wh cm}^{-2}$, respectively. The shape of CV curves deviate from a rectangle and the encapsulated areas also decrease as the increase of scan rates. In GCD tests, GCS shows a capacitance of 208.4 mF cm^{-2} at current density of 1.1 mA cm^{-2} . The corresponding P_A and E_A are $346 \text{ }\mu\text{W cm}^{-2}$ and $14.4 \text{ }\mu\text{Wh cm}^{-2}$, respectively. C_A decreases to 123 mF cm^{-2} under current density of 13.8 mA cm^{-2} . Figure 4c shows the dependence of C_m of GCS, AGF and SGF on scan rates. The calculations based on CV and GCS curves are depicted in Supporting Information, and detailed data are listed in Table S1,2. Figure 4d shows the Nyquist plot from EIS test of GCS, AGF and SGF with frequency ranging from 10 mHz to 0.1 MHz at voltage amplitude of 5 mV. The inset is the magnification of the high frequency region, with an intercept of *ca.* 240 ohm and no semi-circle was observed. The curve can be fitted by an equivalent circuit made of a Warburg open component and a resistance (Figure S7). We suggest that the intercept of *ca.* 240 ohm represents a combined resistance of electrode resistance, solution resistance and charge transfer resistance in this supercapacitor. The resistance is indeed high compared with the traditional supercapacitors, while it is acceptable, considering that GCS is a micro-supercapacitor³². Table S4 shows a comparison on this issue. This drawback may be conquered in the future, for example, more effective reduction methods can be applied to GO assemblies to improve its intrinsic conductivity (the intrinsic conductivity of AGF was measured as 6000 S m^{-1}), or a highly conductive metal wire can be implanted in GCS.¹⁰ GCS is not highly porous compared with the graphene-based aerogel or hydrogel supercapacitors, indicated by its unsatisfying rate performance (Figure 4c) and slop of Nyquist plot at low frequency (Figure 4d). However, GCS obviously surpasses the previously reported wet-spun graphene fiber supercapacitors^{21, 23} in terms of both rate performance and C_m .

It is noteworthy that GCS exhibits a C_m about 1.5 times that of AGF and SGF tested under parallel alignment. The EIS test also demonstrates that GCS holds a smaller resistance than AGF and SGF. Both of them indicate the advantage of the coaxial structure.

As a comparison, C_A of GCS (208.4 mF cm^{-2} at current density of 1.1 mA cm^{-2}) is higher than the CNT/graphene yarn supercapacitor (177 mF cm^{-2} at current density of 0.1 mA cm^{-2} which is the capacitance in terms of single electrode)²³, more than two times the value of the coaxial fiber made by MWNT and carbon nanofibers (86.8 mF cm^{-2} at current density of 0.38 mA cm^{-2})³³, much higher than graphene fiber supercapacitor (9.4 mF cm^{-2})²¹ and a coaxial all-CNT supercapacitor fiber (8.66 mF cm^{-2})²⁹.

The mechanism of EDLC offers it better cycle stability than common pseudocapacitors and batteries. Our GCS shows almost 100% capacitance retention after 10000 times charge and discharge cycles (Figure 4e). A LED was lighted up by pre-charged serially connected GCSs (inset of Figure 4e). (The lit-up voltage of the LED we used is 1.9 to 2.1 V. Thus three GCSs were serially connected and pre-charged to 2.4 V by chronopotentiometry mode in CHI660e.) GCS can also be co-woven with a cotton yarn (insets of Figure 4e). To demonstrate the potential of GCS used as textile electronics, we followed the capacitance retention by CV tests during repeated bending of GCS. The capacitance retention was 92% after 100 bending cycles (Figure 4f).

Organic electrolyte without active proton can effectively increase the working voltage window, thus increasing the energy density, which is more applicable for daily usage. For this purpose, a polymeric electrolyte gel (1-ethyl-3-methylimidazolium tetrafluoroborate (EMIMBF₄)/polyvinylidene fluoride-co-hexafluoropropylene (PVDF)/DMF) was applied in our GCS. As far as we know, this is the first example of organic phase fiber supercapacitor. PVDF/DMF and GO layer were successively dip-coated on AGF to make the separation layer and outer electrode. The coating of both layers is also quite uniform like that in its aqueous counterpart (Figure 5a-c). Figure 5d shows the CV curves for organic GCS (details in Figure S2 and Table S3). The working voltage window here is as large as 2.4 V. The C_A reaches 131 mF cm⁻² at 10 mV/s. The organic GCS proves the versatile usage of our coaxial assembly method for coaxial fiber supercapacitor and allows the application of organic electrolyte in fiber supercapacitors, offering higher energy density to flexible electronics.

The Ragon plot for aqueous and organic GCS derived from CV curves was drawn in Figure 5e at various power densities. The energy density of organic GCS in terms of the surface area of AGF varied from 104 to 13.5 μWh cm⁻² corresponding to a power density from 1570 to 4159 μW cm⁻². Even the energy density of aqueous GCS (17.5 μWh cm⁻² at 819 μW cm⁻²) is higher than the previously reported asymmetric MnO₂/graphene yarn supercapacitor (8.2 μWh cm⁻² at 930 μW cm⁻²)²² and the coaxial MWNT/carbon nanofibers supercapacitor (9.8 μWh cm⁻²)³³, more than 4 times that of polyelectrolyte-coated graphene yarn supercapacitor (3.84 μWh cm⁻²)²³.

Conclusions

In conclusion, we have designed and fabricated a coaxial all-graphene fiber supercapacitor with a continuously LC wet-spun core fiber and a dip-coated cylinder sheath fiber as the two electrodes. The as formed GCS exhibits a high C_A of 204 mF cm⁻², C_L of 4.63 mF cm⁻¹ and C_m of 185 F g⁻¹. Applying organic ion liquid electrode, the energy density was increased to 104 μWh cm⁻². A well-kept capacitance during repeated bending demonstrates the potential of GCS in the area of flexible textile electronics.

Experiment Section

The wet-spinning technique: 8 mg mL⁻¹ GO solution was used as the spinning dope. A coagulation bath was made of 375 mL H₂O, 125 mL ethanol and 25 g CaCl₂. GO solution was spun into the bath by an injection pump. The freshly made gel fibers were washed in water and ethanol mixed solvents (1:1 in volume). The gel fibers were then collected and dried under room temperature for more than 24 hours.

The dip-coating process: (1) Separation layer: AGF was dipped into freshly-made PVA/H₂O for several seconds, and then drawn out to leave in air for several minutes for the solidification of PVA gel. The coating was done for 3 times for a safe separator layer. (2) GO gel layer: PVA-coated AGF was dipped into CaCl₂ solution (5 wt%) and ~25 mg mL⁻¹ GO solution successively, then dipped into 1:1 water and ethanol mixed solvents. The GO gel layer was left for several minutes for solidification. The coating mass can be controlled by the coating cycles or the concentration of GO solution.

Acknowledgement

This work is funded by the National Natural Science Foundation of China (no. 21325417 and no. 51173162).

Notes and references

^a MOE Key Laboratory of Macromolecular Synthesis and Functionalization, Department of Polymer Science and Engineering, Zhejiang University, 38 Zheda Road, Hangzhou 310027, China. E-mail: chaogao@zju.edu.cn

† Electronic Supplementary Information (ESI) available: [Instruments, calculations and Tables of electrochemical test results, etc.]. See DOI: 10.1039/b000000x/

1. Y. Gogotsi, *Nature*, 2014, **509**, 568-570.
2. X. F. Wang, X. H. Lu, B. Liu, D. Chen, Y. X. Tong and G. Z. Shen, *Adv. Mater.*, 2014, **26**, 4763-4782.
3. B. E. Conway, *Electrochemical Supercapacitors: Scientific Fundamentals and Technological Applications*, Kluwer Academic/Plenum Publishers, New York, 1999.
4. Q. Meng, H. Wu, Y. Meng, K. Xie, Z. Wei and Z. Guo, *Adv. Mater.*, 2014, **26**, 4100-4106.
5. Z. Yang, J. Deng, X. Chen, J. Ren and H. Peng, *Angew. Chem. Int. Ed.*, 2013, **52**, 13453-13457.
6. M. Ghidui, M. R. Lukatskaya, M.-Q. Zhao, Y. Gogotsi and M. W. Barsoum, *Nature*, 2014, **516**, 78-81.
7. Y. Meng, Y. Zhao, C. Hu, H. Cheng, Y. Hu, Z. Zhang, G. Shi and L. Qu, *Adv. Mater.*, 2013, **25**, 2326-2331.
8. X. Lu, M. Yu, G. Wang, Y. Tong and Y. Li, *Energ. Environ. Sci.*, 2014, **7**, 2160-2181.
9. Y. He, W. Chen, C. Gao, J. Zhou, X. Li and E. Xie, *Nanoscale*, 2013, **5**, 8799-8820.
10. J. A. Lee, M. K. Shin, S. H. Kim, H. U. Cho, G. M. Spinks, G. G. Wallace, M. D. Lima, X. Lepró, M. E. Kozlov, R. H. Baughman and S. J. Kim, *Nat. Commun.*, 2013, **4**.
11. D. H. Zhang, M. H. Miao, H. T. Niu and Z. X. Wei, *ACS Nano*, 2014, **8**, 4571-4579.
12. K. Wang, Q. Meng, Y. Zhang, Z. Wei and M. Miao, *Adv. Mater.*, 2013, **25**, 1494-1498.
13. H. Sun, X. You, Y. S. Jiang, G. Z. Guan, X. Fang, J. Deng, P. N. Chen, Y. F. Luo and H. S. Peng, *Angewandte Chemie-International Edition*, 2014, **53**, 9526-9531.
14. X. L. Chen, H. Sun, Z. B. Yang, G. Z. Guan, Z. T. Zhang, L. B. Qiu and H. S. Peng, *J. Mater. Chem. A*, 2014, **2**, 1897-1902.

15. Z. T. Zhang, X. L. Chen, P. N. Chen, G. Z. Guan, L. B. Qiu, H. J. Lin, Z. B. Yang, W. Y. Bai, Y. F. Luo and H. S. Peng, *Adv. Mater.*, 2014, **26**, 466-470.
16. Z. Xu, Y. Zhang, P. Li and C. Gao, *ACS Nano*, 2012, **6**, 7103-7113.
17. Z. Dong, C. Jiang, H. Cheng, Y. Zhao, G. Shi, L. Jiang and L. Qu, *Adv. Mater.*, 2012, **24**, 1856-1861.
18. S. H. Aboutalebi, R. Jalili, D. Esrafilzadeh, M. Salari, Z. Gholamvand, S. A. Yamini, K. Konstantinov, R. L. Shepherd, J. Chen, S. E. Moulton, P. C. Innis, A. I. Minett, J. M. Razal and G. G. Wallace, *ACS Nano*, 2014, **8**, 2456-2466.
19. Z. Xu, H. Sun, X. Zhao and C. Gao, *Adv. Mater.*, 2013, **25**, 188-193.
20. H. Cheng, C. Hu, Y. Zhao and L. Qu, *NPG Asia Mater.*, 2014, **6**, e113.
21. T. Huang, B. Zheng, L. Kou, K. Gopalsamy, Z. Xu, C. Gao, Y. Meng and Z. Wei, *RSC Adv.*, 2013, **3**, 23957-23962.
22. B. N. Zheng, T. Q. Huang, L. Kou, X. L. Zhao, K. Gopalsamy and C. Gao, *J. Mater. Chem. A*, 2014, **2**, 9736-9743.
23. L. Kou, T. Q. Huang, B. N. Zheng, Y. Han, X. L. Zhao, K. Gopalsamy, H. Y. Sun and C. Gao, *Nat. Commun.*, 2014, **5**.
24. K. Gopalsamy, Z. Xu, B. Zheng, T. Huang, L. Kou, X. Zhao and C. Gao, *Nanoscale*, 2014, **6**, 8595-8600.
25. Z. Xu and C. Gao, *Acc. Chem. Res.*, 2014, **47**, 1267-1276.
26. B. Zheng and C. Gao, *Chin. Polym. Bull.*, 2013, **10**, 171-178.
27. Y. Meng, Y. Zhao, C. Hu, H. Cheng, Y. Hu, Z. Zhang, G. Shi and L. Qu, *Adv. Mater.*, 2013, **25**, 2326-2331.
28. Y. Hu, H. H. Cheng, F. Zhao, N. Chen, L. Jiang, Z. H. Feng and L. T. Qu, *Nanoscale*, 2014, **6**, 6448-6451.
29. X. Chen, L. Qiu, J. Ren, G. Guan, H. Lin, Z. Zhang, P. Chen, Y. Wang and H. Peng, *Adv. Mater.*, 2013, **25**, 6436-6441.
30. J. Zou and F. Kim, *Nat. Commun.*, 2014, **5**, 5254.
31. M. D. Stoller and R. S. Ruoff, *Energ. Environ. Sci.*, 2010, **3**, 1294-1301.
32. D. Harrison, F. Qiu, J. Fyson, Y. Xu, P. Evans and D. Southee, *Phys. Chem. Chem. Phys.*, 2013, **15**, 12215-12219.
33. V. T. Le, H. Kim, A. Ghosh, J. Kim, J. Chang, Q. A. Vu, D. T. Pham, J.-H. Lee, S.-W. Kim and Y. H. Lee, *ACS Nano*, 2013, **7**, 5940-5947.

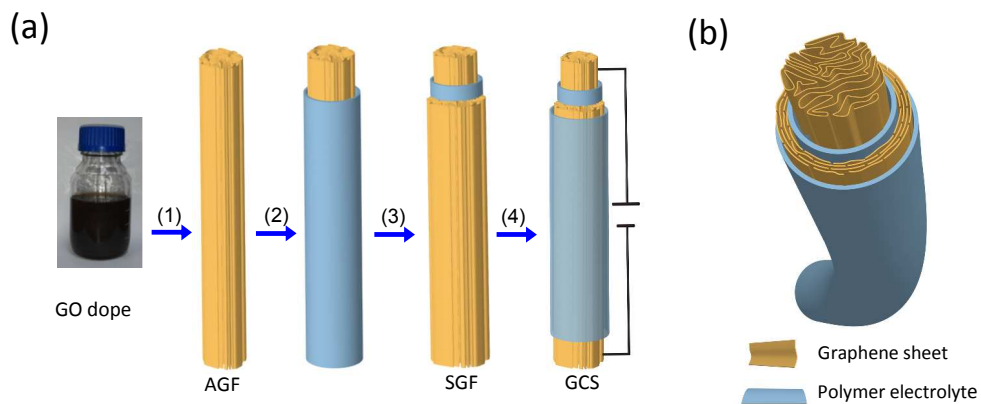


Fig. 1 Schematic illustration for (a) the fabrication process and (b) the cross section structure of a GCS with a core fiber and a cylinder sheath as the two electrodes. (1) wet-spinning and chemical reduction. (2) dip-coating of polymer electrolyte gel. (3) dip-coating of GO gel and chemical reduction. (4) dip-coating of polymer electrolyte gel.

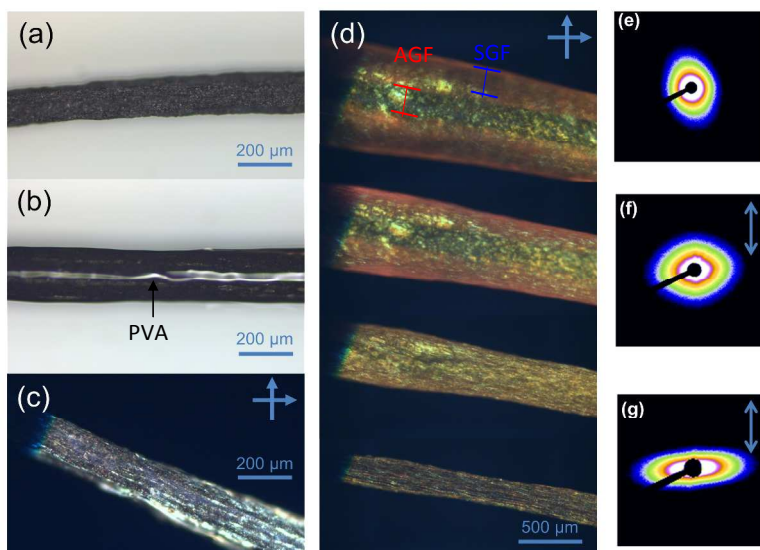


Fig. 2 Microscopic images of AGF (a), PVA gel-coated AGF (b,c), the GO gel-coated fiber and the shrinking process (d). (c, d) were taken between crossed polarizers. 2D SAXS patterns of the original concentrated GO dispersion as the wet-spinning dope (e), the gel state axial fiber (f) the gel state GO coating layer (g). Note that the 2D SAXS pattern of solid AGF does not show asymmetry under the same condition. The inset arrows in (f) and (g) indicate the fiber arrangement direction. The inset red and blue marks indicate AGF and the dip-coated GO layer (precursor of SGF), respectively.

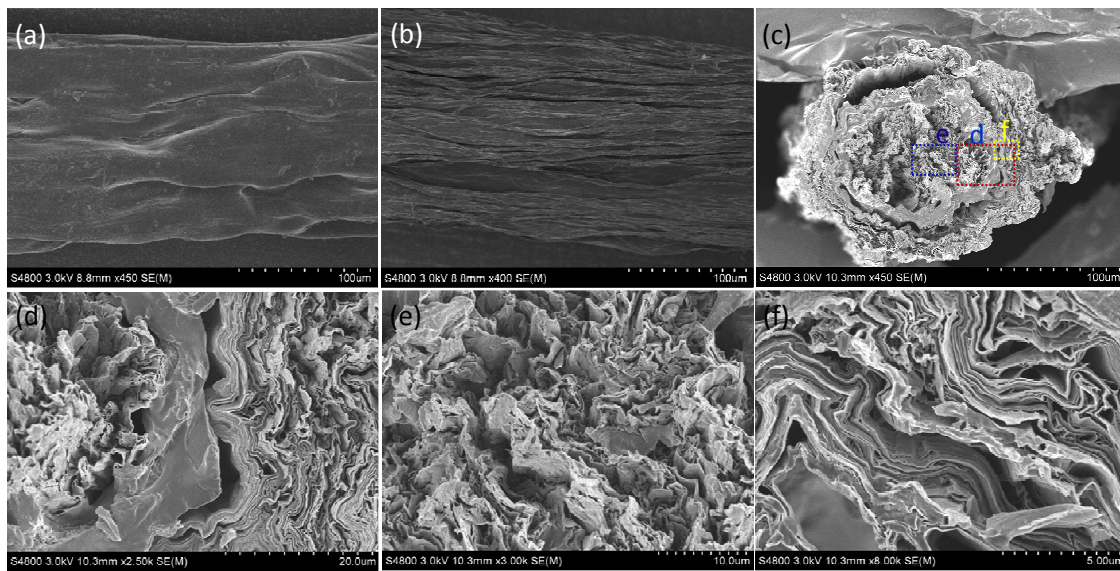


Fig. 3 SEM images of the side view of PVA-coated AGF (a), GCS without the outer gel electrolyte (b), (c-f) the cross section images of a GCS without the outer gel electrolyte at different magnitudes. Images in (d-f) are the magnifications of the red, blue and yellow frame-marked regions in (c).

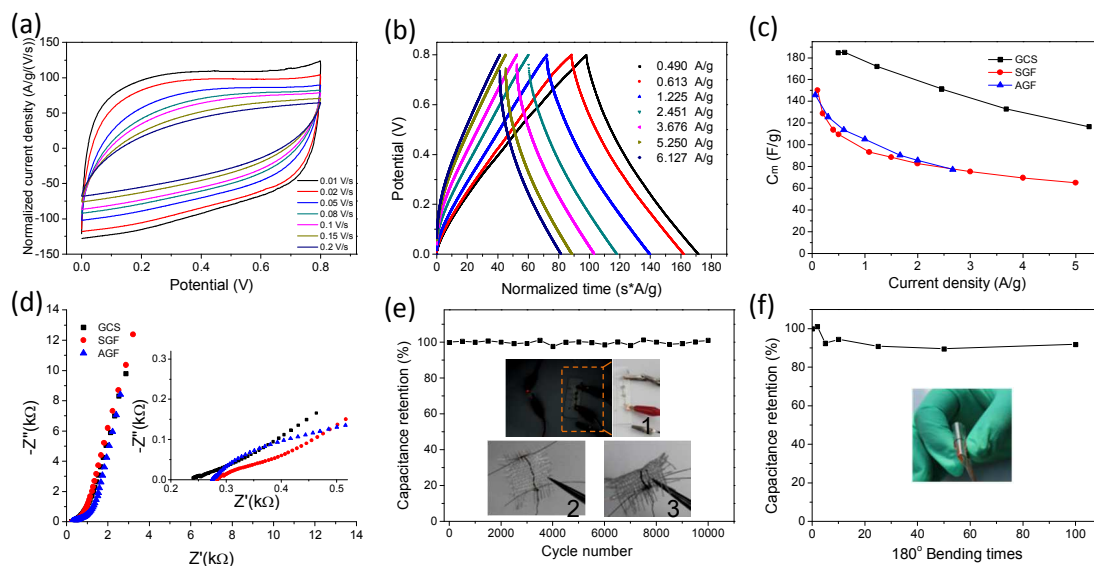


Fig. 4 Electrochemical performance of GCS. (a) CV curves at different voltage scan rates. The current density is normalized by the scan rates in the scanning. (b) GCD curves at different current density from 0.49 A g^{-1} (1.1 mA cm^{-2}) to 6.13 A g^{-1} (13.8 mA cm^{-2}). The charge and discharge time is normalized by the current densities. (c) C_m of GCS, AGF and SGF at different current densities obtained from GCD test. (d) Nyquist plot from EIS test for GCS, AGF and SGF. The inset is the magnification of the high frequency region. (e) Long cycle capacitance retention of GCS at current density of 5.56 mA cm^{-2} . The inset 1 is a LED lighted up by pre-charged serially-connected GCSs. The inset 2 and 3 are photos of GCS in cotton textile. (f) Capacitance retention of GCS under 100 times of bending. The inset photo displays the 180° bending state.

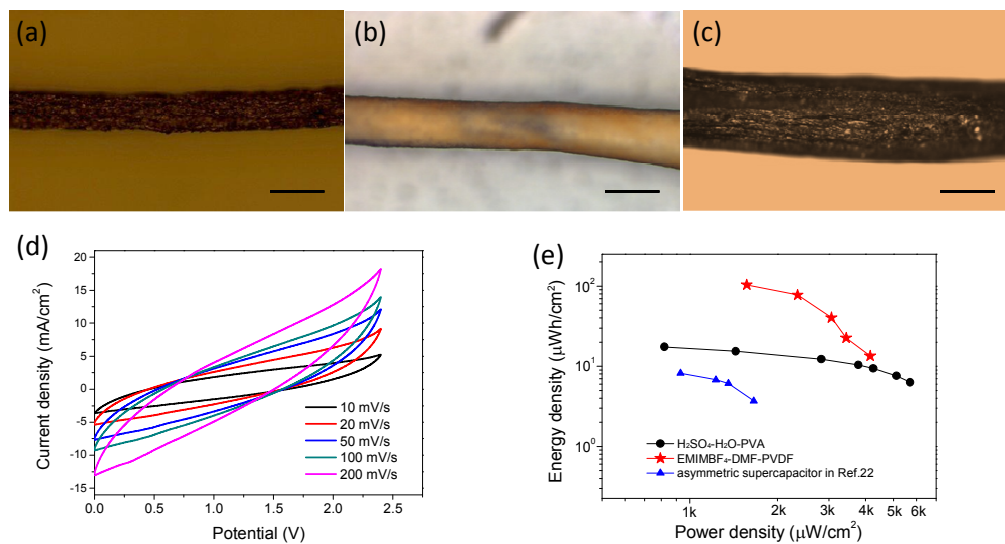


Fig. 5 Microscopic images of (a) AGF (b) PVDF-coated AGF (c) GCS without the outer gel electrolyte. (d) CV curves for organic phase GCS at a voltage window of 2.4 V. (e) Ragon plot of aqueous phase GCS, organic phase GCS and an asymmetric fiber supercapacitor from Ref. 22. The scale bars in (a-c) are 200 μm .